DECEMBER 1990 ECN-RX--90-096

NL91C0695

POSITRON-ANNIHILATION 2D-ACAR MEASUREMENTS IN THE INCOMMENSURATELY MODULATED HIGH-T_c SUPERCONDUCTOR $Bi_2Sr_2CaCu_2O_{8+x}$

P.E. MIJNARENDS
A.F.J. MELIS
A.W. WEEBER
A.A. MENOVSKY*
K. KADOWAKI*

* NATUURKUNDIG LABORATORIUM DER UNIVERSITEIT VAN AMSTERDAM, VALCKENIERSTRAAT 65, 1018 XE AMSTERDAM, THE NETHERLANDS

* PRESENT ADDRESS: NATIONAL RESEARCH INSTITUTE FOR METALS, TSUKUBA, IBARAKI 305, JAPAN

TO BE PUBLISHED IN PHYSICA C

The Netherlands Energy Research Foundation ECN is the leading institute in the Netherlands for energy research. ECN carries out pure and applied research in the fields of nuclear energy, fossil fuels, renewable energy sources, environmental aspects of energy supply, computer science and the development and application of new materials. Energy studies are also a part of the research programme.

ECN employs more than 900 staff. Contracts are obtained from the government and from national and foreign organizations and industries.

ECN's research results are published in a number of report series, each series serving a different public from contractors to the international scientific world.

This RX-series is used for publishing pre-prints: the preliminary versions of articles that will appear in a journal, or conference or symposium proceedings. Please do not refer to this report but use the reference provided on the title page: 'To appear in ...' or 'Submitted for publication to ...'.

The Netherlands Energy Research Foundation ECN
Scientific and Technical Information Department
P.O. Box 1
NL-1755 ZG Petten
The Netherlands
Telephone: +31 2246 4323
Fax : +31 2246 3483

This report is available on remittance of Dfl. 20 to:
ECN, TWI Department,
Petten, The Netherlands.
Giro account (postal account) No. 3977703.
Please quote the report number.

POSITRON-ANNIHILATION 2D-ACAR MEASUREMENTS IN THE INCOMMENSURATELY MODULATED HIGH-T_c SUPERCONDUCTOR $Bi_2Sr_2CaCu_2O_{8+x}$

P.E. Mijnarends[1], A.F.J. Melis[1], A.W. Weeber[1], A.A. Menovsky[2] and K. Kadowaki[2*]

[1] Materials Unit, Netherlands Energy Research Foundation ECN, 1755 ZG Petten, The Netherlands

[2] Natuurkundig Laboratorium der Universiteit van Amsterdam, Valckenierstraat 65, 1018 XE Amsterdam, The Netherlands

[*] Present address: National Research Institute for Metals, Tsukuba, Ibaraki 305, Japan

Keywords: positron annihilation
modulated structures
electronic structure
$Bi_2Sr_2CaCu_2O_{8+x}$

Petten, November 1990

ABSTRACT

Measurements are presented of the two-dimensional angular correlation of annihilation radiation (2D-ACAR) in a single crystal of approximate composition $Bi_2Sr_2CaCu_2O_{8+x}$ (T_c = 85 K) at 6 K and 92 K. Data taken with projection along the c axis show a strong C_{2v} symmetry due to the presence of an incommensurate modulation with wave vector $\underset{\sim}{q}$ in the crystal structure, together with considerable fine-structure. It is shown theoretically that the modulation should cause images of the Fermi surface displaced over an integer times $\underset{\sim}{q}$ relative to the usual high-momentum components. An analysis of the behaviour of the fine-structure in the 2D-ACAR distribution shows that many peaks change in intensity and width but little in position as T is raised from 6 to 92 K.

1. INTRODUCTION

Among the materials with a high superconducting transition temperature T_c, the compounds with the general formula $Bi_2Sr_2(CaCuO_2)_nCuO_6$ (with n=0,1,2,...) take a prominent position since T_c increases as the number of $CaCuO_2$ layers increases from zero to two. Also, it proves relatively easy to grow good quality single crystals of the n=1 phase (T_c about 85 K) which are largely free of other phases. The structure of $Bi_2Sr_2CaCu_2O_8$ consists essentially of two CuO_2 layers separated by an oxygen deficient Ca layer. This (CuO_2-Ca-CuO_2) package is sandwiched between two BiO layers and separated from these by SrO layers [1]. The terminating BiO layers of successive structural units are relatively far apart (3.2 Å) and hence form natural cleavage planes [2].

The crystallographic unit cell of $Bi_2Sr_2CaCu_2O_{8+x}$ has been determined to be orthorhombic with lattice parameters a = 5.414, b = 5.418, and c = 30.89 Å [1]. It can be described as derived from a body-centered tetragonal parent structure with a' = b' = 3.83 A. The structure is complicated by the occurrence of an incommensurate lattice modulation along the b axis with a period of 4.76 b, caused by the insertion of extra oxygen atoms in the BiO layers (leading to an excess oxygen content indicated by $x > 0$ in the chemical formula) accompanied by a relaxation of the surrounding atoms [3-5]. This modulation has also been described as originating in the absence of a row of Bi atoms every nine or ten atomic sites in combination with a displacive modulation of the Bi atoms [6].

Band-structure calculations have been performed by a number of authors (e.g., refs. [7,8]) on the basis of the parent tetragonal structure, and by Massidda et al. [9] for the face-centered orthorhombic structure, assuming the applicability of the local density approximation to these materials. The calculations result in a Fermi surface consisting of two large concentric nearly-degenerate Cu-O-plane-related hole sheets centered at the zone corners having low dispersion along the [001] axis, and small electron pockets around the L point and halfway Γ and Z, related to Bi-O bands. These electron pockets reduce the filling of the Cu-O bands, thus effectively doping the Cu-O bands with extra holes [10] and promoting superconductivity. Herman et al. [11] have shown however that, as expected, the Bi-O bands are quite sensitive to the exact arrangement of the O atoms in the Bi-O layers.

Experimental information about the electronic structure of this compound has been obtained by optical [12,13] and photoemission spectroscopy [14-17] and therefore is mostly related to the density of states. Data pertaining to the dispersion in $\underset{\sim}{k}$ space have been obtained using angle-resolved photoemission [18]. Other $\underset{\sim}{k}$-related information may be obtained from a measurement of the two-dimensional angular correlation of annihilation radiation (2D-ACAR) $N(p_y,p_z)$ from thermalized positrons [19], given by

$$N(p_y,p_z) = \text{const.} \int \rho(\underset{\sim}{p})\, dp_x, \qquad (1)$$

where $\rho(\underset{\sim}{p})$ denotes the distribution in momentum space of the annihi-

lation photon pairs, given by

$$\rho(\underline{p}) = \sum_{occ} |\chi(\underline{p})|^2 = \sum_{occ} \left|\int \exp(-i\underline{p}.\underline{r})\psi(\underline{r})\phi(\underline{r})d\underline{r}\right|^2 \quad . \qquad (2)$$

Here ψ and ϕ denote the electron and positron wave function respectively and the summation extends over all occupied electron states. Due to momentum conservation, $\rho(\underline{p})$ equals the momentum distribution of the electrons in the solid as sampled by the positron (e^+), and hence its measurement in the once-integrated form (1) yields information about the electronic structure. Recently, Chan et al. [20] have reported 2D-ACAR measurements on single crystals of $Bi_2Sr_2CaCu_2O_{8+x}$, but details have not yet been published. Singh et al. [21] have calculated the e^+ distribution for the idealized structure of $Bi_2Sr_2CaCu_2O_8$. They found that, if positron-electron correlation is included, the positron becomes a better probe of the Cu-O planes, which are thought to play a key role in high-T_c superconductivity. Yet, a substantial fraction of the e^+ density is found between the Bi-O layers due to the preference of the positron for open volumes. The preference for the Bi-O layers may be reinforced by the modulation, which results in regions which are dilute in Bi atoms. Certain is that the e^+ distribution in the crystal lattice will affect the 2D-ACAR distribution significantly.

In the present paper 2D-ACAR measurements on a sample with the approximate composition $Bi_2Sr_2CaCu_2O_{8+x}$ are reported. We make no attempt to interpret these data in terms of a Fermi surface for two reasons. Firstly, previous work on superconducting $YBa_2Cu_3O_7$ [22,23]

has shown that for a reliable separation of Fermi-surface and e^+ wave-function effects it is helpful, if not indispensable, to have some insight in the manner in which the positron wave function affects the momentum distribution. Secondly, as will be shown in the following section, an incommensurate modulation with a displacive component, such as found in $Bi_2Sr_2CaCu_2O_{8+x}$, causes electron states characterized by a wave vector $\underset{\sim}{k}$ to contribute to the momentum density $\rho(\underset{\sim}{p})$ not only at momenta $\underset{\sim}{p} = \underset{\sim}{k} + \underset{\sim}{G}$ (with $\underset{\sim}{G}$ being a vector of the reciprocal lattice) as in ordinary crystals, but also at $\underset{\sim}{p} = \underset{\sim}{k} + \underset{\sim}{G} + m\underset{\sim}{q}$, where m is an integer number times the wave vector $\underset{\sim}{q}$ of the modulation. This gives rise to 'satellite Fermi surfaces' in the momentum density which will complicate the analysis of the data. At present, no momentum density calculations are available for this material, and hence we rather focus on the effects of the crystal structure on the momentum density and their temperature dependence.

2. POSITRON ANNIHILATION IN A MODULATED STRUCTURE

In nature there are many crystals in which the lattice is modulated with a period which is incommensurate with the lattice parameters. Such crystals do not show translational symmetry, and hence do not possess a three-dimensional space group; nevertheless, their diffraction patterns display sharp spots which imply a perfect long-range order. It has been shown by de Wolff [24] and by Janner and Janssen [25] (for a review see ref. [26] and references therein) that for these crystals it is possible to define a higher-dimensional superspace in which lattice periodicity is restored. We shall make use of

this approach to study the momentum density in incommensurately modulated crystals.

Consider a three-dimensional crystal with a basic structure spanned by the vectors $\underset{\sim}{a}$, $\underset{\sim}{b}$, $\underset{\sim}{c}$, and containing a d-dimensional displacive modulation characterized by a wave vector $\underset{\sim}{q}$. In the special case d = 1, the position $\underset{\sim}{r}(\underset{\sim}{n}_j)$ of an atom at $\underset{\sim}{r}_j$ in cell $\underset{\sim}{n}$ is given by

$$\underset{\sim}{r}(\underset{\sim}{n}_j) = \underset{\sim}{n} + \underset{\sim}{r}_j + \underset{\sim}{f}_j(\underset{\sim}{q}.\underset{\sim}{n}), \quad \text{with } f_j(x + 2\pi) = f_j(x). \tag{3}$$

By introducing t, the phase of the modulation, and treating it as a fourth variable in addition to the vectors $\underset{\sim}{a}$, $\underset{\sim}{b}$, $\underset{\sim}{c}$, the three-dimensional (3D) crystal can be considered imbedded in a four-dimensional (4D) superspace. In this configuration space a perfectly periodic four-dimensional lattice Σ can be defined. An atomic position in Σ is given by

$$[\underset{\sim}{r}(\underset{\sim}{n}_j), t] = [\underset{\sim}{n} + \underset{\sim}{r}_j + \underset{\sim}{f}_j(\underset{\sim}{q}.\underset{\sim}{n} + t), t], \tag{4}$$

and Σ is left invariant under the four translations

$$a_1 = (\underset{\sim}{a}, -\underset{\sim}{q}.\underset{\sim}{a}), \; a_2 = (\underset{\sim}{b}, -\underset{\sim}{q}.\underset{\sim}{b}), \; a_3 = (\underset{\sim}{c}, -\underset{\sim}{q}.\underset{\sim}{c}), \quad \text{and } a_4 = (0, 2\pi), \tag{5}$$

which together span the four-dimensional lattice. The original 3D crystal is retrieved by setting t = 0, i.e., it is obtained by intersecting the 4D lattice with the hyperplane t = 0. A three-dimensional modulated lattice which can be considered as an imbedding in a perfectly periodic higher-dimensional lattice is called quasi-periodic.

A lattice Σ^* reciprocal to Σ is defined by the vectors

$$b_1 = (\underset{\sim}{a}^*,0), \quad b_2 = (\underset{\sim}{b}^*,0), \quad b_3 = (\underset{\sim}{c}^*,0), \text{ and } b_4 = (\underset{\sim}{q},1). \tag{6}$$

It is easily verified that with this choice of direct and reciprocal vectors

$$(a_i.b_j) = 2\pi\,\delta_{ij}. \tag{7}$$

i.e., Σ^* is indeed reciprocal to Σ. An arbitrary vector in Σ^* can then be written as $(h\underset{\sim}{a}^* + k\underset{\sim}{b}^* + l\underset{\sim}{c}^* + m\underset{\sim}{q}, m)$. The modulation is called incommensurate if $\underset{\sim}{q}$ does not have a multiple belonging to the basic reciprocal lattice spanned by $\underset{\sim}{a}^*$, $\underset{\sim}{b}^*$, and $\underset{\sim}{c}^*$.

In order to calculate the momentum density $\rho(\underset{\sim}{p})$ given by (2) for band electrons in an incommensurate crystal, the Schrödinger equation must be solved for the electrons and the positron. For the sake of brevity and clarity we concentrate on the role played by the electron and assume a constant e^+ wave function. Following de Lange and Janssen [27] we formulate the Schrödinger equation for an electron in the quasi-periodic potential $V(\underset{\sim}{r})$, which is considered as the restriction to three-dimensional space of a potential $V(\underset{\sim}{r},t)$ possessing lattice periodicity in 4D superspace. The kinetic energy is represented by a Laplace operator in threedimensional space; thus

$$[-(\hbar^2/2m)\nabla^2 + V(\underset{\sim}{r},t)]\,\psi(\underset{\sim}{r},t) = E(t)\,\psi(\underset{\sim}{r},t). \tag{8}$$

For incommensurate crystals E(t) can be shown to be independent of t [27].

Since $V(\underline{r},t)$ is periodic in four dimensions, the wave function ψ may be written in the Bloch form

$$\psi(\underline{r},t) = \exp(i\underline{k}_s.\underline{r}_s)\, U(\underline{r}_s), \tag{9}$$

where $\underline{k}_s$ denotes the 4D wave vector $(\underline{k},k_4)$ and $\underline{r}_s$ the position vector $(\underline{r},t)$. The function $U(\underline{r}_s)$ has the full lattice periodicity in 4D and hence has a 4D Fourier expansion

$$U(\underline{r}_s) = \sum_{\underline{K}_s} u(\underline{K}_s) \exp(i\underline{K}_s.\underline{r}_s), \tag{10}$$

where $\underline{K}_s$ is a reciprocal lattice vector in Σ^*. Because of the 3D character of the kinetic energy term the factor $\exp(ik_4.t)$ cancels in the Schrödinger equation, and the 3D wave function $\psi(\underline{r})$ obtained by setting $t = 0$ becomes

$$\psi(\underline{r}) = \exp(i\underline{k}.\underline{r})\, U(\underline{r},0), \tag{11}$$

i.e., it may be viewed as the restriction of $\psi(\underline{r},t)$ to the three-dimensional space of the physical crystal. It is now possible to perform the Fourier transform in (2), using eqs. (9)-(11) and remembering that we have set $\Phi = 1$:

$$\chi(\underline{p}) = \int d\underline{r}\, \exp(-i\underline{p}.\underline{r})\, \psi(\underline{r}) = \int d\underline{r}\, \exp[-i(\underline{p}-\underline{k}).\underline{r}]\, U(\underline{r},0)$$

$$= \int dp_4 \int dr_s \sum_{K_s} u(K_s) \exp[-i(p_s - k_s - K_s).r_s]. \qquad (12)$$

In the second line of (12) use has been made of a theorem which states that the projection of the Fourier transform of a function f, defined in an n-dimensional Euclidian space R^n, onto a subspace R^m ($m < n$) equals the Fourier transform of the restriction of f to R^m (for a proof see ref. [26]). Performing the integration with respect to r_s yields

$$\chi(p) = (2\pi)^3 \int dp_4 \sum_{K_s} u(K_s) \delta(p - k - K) \delta(p_4 - k_4 - K_4). \qquad (13)$$

Since $K_s = (G + mq, m)$ [where G is a vector in the basic reciprocal lattice spanned by b_1, b_2, and b_3 defined in (6)] and $k_4 = 0$, the projection along p_4 causes a summation over m, and hence

$$\chi(p) = (2\pi)^3 \sum_{G} \sum_{m} u(G + mq, m) \delta(p - k - G - mq). \qquad (14)$$

Equation (14) states that an electron with wave vector k contributes to the momentum density at momenta $p = k + G + mq$. Thus, in addition to the well-known higher momentum components (HMC) [19,28] for $m = 0$, the incommensurate modulation results in satellite contributions around each HMC for which $m \neq 0$. This situation is very similar to the satellite reflections found in diffraction diagrams. The summation over all occupied electron states in (2) causes the momentum distribution to reflect the geometry of the Fermi surface. The occurrence of the satellites should produce 'images' of the Fermi surface shifted over a distance mq in momentum space, thereby making the re-

lation between the positron-electron momentum density and the Fermi-surface of an incommensurately modulated material more complex than in unmodulated materials.

3. EXPERIMENT

The measurements were performed on an unannealed platelet-shaped single crystal with dimensions 3.5 × 2.5 × 0.05 mm^3, obtained by cleaving from the boule, which was grown by the travelling solvent floating zone method [29] using a NEC infrared image furnace. Small-focus Laue x-ray transmission and back-reflection photographs, as well as neutron diffraction rocking scans through the (200), (020) and (002) reflections showed the crystal to be of a good quality. The latter measurements revealed a mosaic distribution of crystallites with the a axes oriented parallel within the instrumental resolution of 0.23°. Rocking the crystal through the (002) reflection about this common [100] direction yielded an asymmetric intensity profile with a full width at half maximum of 0.58° and a small side peak with a resolution-limited width (fig. 1). The anguiar spread of the c axes, and consequently of the b axes as well, is probably caused by the intergrowth of extra layers in a part of the crystal. AC susceptibility measurements gave a single sharp transition with an onset at T = 85 K and midpoint at 79.4 K without any signals at higher T, while also high-resolution microscopic analysis on a sample from the same batch did not reveal other phases.

2D-ACAR measurements with integration along the c axis were performed at T = 6 K and 92 K with a setup employing high-density multiwire

proportional chambers [30]. These temperatures are measured at the base of the sample mount; the actual temperature of the sample which faces the Ti window through which the e^+ beam enters the cryostat may be somewhat higher. The sample, attached with an epoxy glue to a 20 μm thick Au-plated W wire strung between two supports and placed, together with the source, in a 6 Tesla magnetic field to guide the positrons, was not moved between the two measurements. As a result of the strong diamagnetism in the sample below T_c and its highly 2D morphology, the sample is self-orientating in a measurement with $T < T_c$ and c-axis integration. The sample-detector distance was ~ 8 m, resulting in an estimated total resolution of ~ 0.6 × 0.6 $mrad^2$ at 6 K (1 mrad = 10^{-3} mc = 0.137 a.u. of momentum), and somewhat worse at 92 K. The source consisted of ~ 2.2 GBq ^{22}Na. Data were taken on a 600 × 600 mesh with a channel width of 0.125 mrad. At 6 K about 20 × 10^6 counts were collected, during the measurements at 92 K about 14 × 10^6.

As is common for materials with a complex band structure with many filled bands, the 2D-ACAR distributions after correction for the instrumental momentum sampling function [31] show a high amount of isotropy. The anisotropy may be brought out by subtraction of a heavily smoothed isotropic distribution which lies everywhere below the measured distribution. The remainder is the anisotropy, which is shown in fig. 2 for the 6 K measurement with c-axis integration, after gaussian smoothing with a full width at half maximum of 0.375 mrad. The striking aspect of this figure is the absence of the C_{4v} symmetry which would have corresponded to the parent tetragonal structure of the material. Instead, the underlying data display an approximate C_{2v} symmetry [32], which has been used to symmetrize the

data to improve statistics. The height of the two highest peaks in fig. 2 is 4.1 % of that of the total distribution at $(p_y,p_z) = (0,0)$ (the x direction being the direction of integration). The anisotropy consists essentially of four peaks. The two peaks on the $\underset{\sim}{a}^*$ axis are elongated in the $\underset{\sim}{b}^*$ direction; the two peaks on the $\underset{\sim}{b}^*$ axis are split. At higher momenta 'echos' of these peaks are seen on both axes. The 'echo' on the $\underset{\sim}{a}^*$ axis lies at a momentum twice that of the main peak; along the $\underset{\sim}{b}^*$ axis a similar relationship between the main and secondary peaks is not as clear.

In order to check whether the mounting material contributes to the anisotropy, a separate spectrum has been taken of the W wire carrying a drop of epoxy glue roughly the same size as used in the actual mounting of the sample. A total of 0.7×10^6 coincidences was recorded in 18 % of the time spent on the measurement with the sample at 6 K. This spectrum was isotropic without any sign of C_{2v} anisotropy, while the measurement with the sample in place showed already a pronounced anisotropy after the same counting time.

Figures 3a and 4a show cuts through the smoothed 2D-ACAR distribution at 6 K along the $\underset{\sim}{a}^*$ and $\underset{\sim}{b}^*$ axes respectively. In order to improve statistics, each curve represents the sum of five adjacent rows of channels, i.e., a strip 0.625 mrad wide. The error bars include all covariances between data points resulting from translation, rotation, smoothing and row addition. The curves are shown before symmetrization to allow an assessment of their symmetry. The most remarkable feature is the presence of a number of relatively narrow, often overlapping peaks. The width of some of these peaks is less than 1 mrad.

i.e., their width is comparable to the instrumental resolution. In order to facilitate the analysis the peaks have been labeled by the channel number with respect to the origin. The cut along p_y (fig. 3a), where p_y points along the $\underline{a}^*$ direction, shows two large peaks at ± 5.3 mrad with a full width at half maximum (FWHM) of about 2.3 mrad. The 'echos' at twice these momenta are clearly visible. A careful consideration of the slopes of the two large peaks suggests that they overlap with smaller peaks, but the extent of the overlap is such that the exact position of the latter is hard to establish. Between the large peaks a few smaller peaks are seen. The positions and intensities of these are not quite symmetric with respect to p_y = 0, but since they are also found in the 92 K measurements (see below) their existence is beyond doubt. It is however possible that effects of the mounting (W wire and epoxy glue) affect the spectrum and perturb its symmetry in the low momentum region. Along the p_z axis (fig. 4a), the modulation direction, there are two fairly broad regions of excess momentum which are each split into three or four main peaks. The outer two are located at ± 5.5 mrad; other peaks are found at about ± 2.0, ± 3.0 and ± 3.8 mrad. There is a suggestion of echos of the outer peaks at twice the momentum, but they are certainly not as clear as those on the p_y axis. A narrow peak at - 0.63 mrad seems to have only a very weak equivalent on the positive side.

The measurement has been repeated at 92 K, i.e., above T_c; the corresponding cuts along the $\underline{a}^*$ and $\underline{b}^*$ axes are shown in figs. 3b and 4b. After correction for the different numbers of total counts in the spectra these cuts show roughly the same amplitude, but there are remarkable changes in structure, which will be discussed in the following section.

4. DISCUSSION

In discussing the differences between the spectra measured at 6 K and 92 K we focus first on the $\underset{\sim}{a}^*$-axis cuts. Comparing fig. 3b with fig. 3a it is seen that the 'echos' of the large peaks at ± 5.3 mrad on the p_y axis at ± 10.6 mrad in fig. 3b appear washed out to some extent; on the other hand, the structure on the slopes of the large peaks has become much more pronounced. Shoulders on these peaks, which were hardly discernible at 6 K, have now developed into clearly present features, suggesting that at 6 K the large peaks were in fact built up from a number of smaller, relatively narrow, peaks. A comparison of the peak positions between figs. 3a and 3b shows that these hardly change; the increase in structure seems rather to be due to a narrowing of several of the peaks as the temperature is raised above T_c.

Turning to the $\underset{\sim}{b}^*$-axis cuts (figs. 4a and 4b), it is clear that the anisotropy along the p_z direction is quite different from that along p_y. Instead of two large peaks one sees a collection of very narrow peaks of comparable height. The positions of many of these peaks hardly seem to change between 6 and 92 K, but their relative amplitudes do. Thus, the peaks at p_z = ± 3.1 mrad seem to grow in amplitude with respect to the neighbouring peaks at ± 3.75 and ± 5.5 mrad when the temperature is raised from 6 to 92 K. Secondly, the weak structure which at 6 K is hardly visible at 0.88 mrad grows considerably when T is raised to 92 K, while on the negative side a narrow peak develops at - 1.1 mrad. On the right hand slope of the latter a remnant is seen of the peak at - 0.63 mrad in the 6 K data.

Let us now consider the overall anisotropy displayed in fig. 2. Since the Brillouin-zone boundaries intersect the $\underset{\sim}{a}^*$ axis at $\pm$ 4.482 mrad, the large peaks are mostly situated in the higher Brillouin zones with a small overlap into the first zone. In the extended zone scheme this is the position of the large nearly-degenerate hole sheets centered at the point X in the band-structure calculation of Massidda et al. [9]. Similarly, the positive regions on the $\underset{\sim}{b}^*$ axis roughly coincide in position with the Y-centered hole sheets. The positions of the electron sheets halfway X-Y on the other hand correspond to saddle points between the major peaks in the anisotropy. Hence, it is not likely that the observed anisotropy in first instance is determined by the Fermi-surface geometry. Positron and electron wave function effects affecting the overlap integral in (2) are probably more important. This is also borne out by the pronounced C_{2v} symmetry of the momentum distribution. Moreover, the observation that the 'echos' of the peaks on the $\underset{\sim}{a}^*$ axis lie at a distance from the origin twice that of the main peaks, rather than shifted over a reciprocal lattice vector, suggests that those echos are not due to higher momentum components of the positron-electron Bloch waves but more likely result from the oscillations in the Fourier-transformed wave functions.

On the other hand, it is unlikely that the experimental data can be explained on the basis of wave-function effects alone. The narrow peaks in the cuts displayed in figs. 3 and 4, and particularly the structure emerging in the peaks on the $\underset{\sim}{a}^*$ axis when $T > T_c$, seem too sharp to be explained by wave-function oscillations in momentum space and suggest Fermi-surface effects. As seen above, a naive attempt at a straightforward correlation of the measured anisotropy with the

theoretical Fermi surface is unsuccessful. Momentum density calculations for some simplified model of the compound, when available, might allow an assessment of the relative importance of Fermi-surface and wave-function effects and hence facilitate such a correlation. However, the inhomogeneity of the e^+ distribution in the crystal in combination with the existence of satellite Fermi-surface images shifted along the $\underline{b}^*$ axis by 0.21 of a Brillouin zone diameter (or a multiple of that distance) will severely complicate such a simple picture. As long as no information exists with regard to the relative strength of the fundamental ($m=0$) and satellite ($m\neq 0$) Fermi-surface images in the electron-positron momentum distribution it is not possible to draw conclusions concerning the manner in which the momentum density reflects the Fermi surface. Computations of the positron wave function, the electronic structure, and the positron-electron momentum density in models which approximate the incommensurately modulated structure of $Bi_2Sr_2CaCu_2O_{8+x}$ as closely as possible would therefore be of great interest.

In summary, we have measured the 2D-ACAR distribution in a single crystal of $Bi_2Sr_2CaCu_2O_{8+x}$ at 6 K and above T_c with projection along the c axis. The distribution shows a pronounced C_{2v} symmetry due to the incommensurately modulated crystal structure. It is shown how such a modulation can affect the way in which the 2D-ACAR distribution reflects the Fermi surface. There is considerable fine-structure and its behaviour under the change of temperature is analysed. In the absence of momentum density calculations no attempt is made to interpret the observed structure in terms of a Fermi surface.

ACKNOWLEDGMENTS

We are indebted to E. Frikkee for performing the neutron measurements on our crystal and to A. Bansil, L.C. Smedskjaer and W.G. Haije for discussions. Thanks are due to G.H. Dai for assistance in preparing the figures, and to G.J. Langedijk for technical assistance. This work is part of the research program of the Stichting Fundamenteel Onderzoek der Materie (Foundation for Fundamental Research on Matter) and was made possible by financial support from the Nederlandse Organisatie voor Wetenschappelijk Onderzoek (Netherlands Organisation for the Advancement of Research).

REFERENCES

[1] S.A. Sunshine, T. Siegrist, L.F. Schneemeyer, D.W. Murphy, R.J. Cava, B. Batlogg, R.B. van Dover, R.M. Fleming, S.H. Glarum, S. Nakahara, R. Farrow, J.J. Krajewski, S.M. Zahurak, J.V. Waszczak, J.H. Marshall, P. Marsh, L.W. Rupp Jr and W.F. Peck, Phys. Rev. B 38 (1988) 893.

[2] P.A.P. Lindberg, I. Lindau and W.E. Spicer, Phys. Rev. B 40 (1989) 6822.

[3] Y. Le Page, W.R. McKinnon, J.-M. Tarascon and P. Barboux, Phys. Rev. B 40 (1989) 6810.

[4] E.A. Hewatt, J.J. Capponi and M. Marezio M, Physica C 157 (1989) 502.

[5] A. Yamamoto, M. Onoda, E. Takayama-Muromachi, F. Izumi, T. Ishigaki and H. Asano, Phys. Rev. B 42 (1990) 4228.

[6] M.D. Kirk, J. Nogami, A.A. Baski, D.B. Mitzi, A. Kapitulnik, T.H. Geballe and C.F. Quate, Science 242 (1988) 1673.

[7] H. Krakauer and W.E. Pickett, Phys. Rev. Lett. 60 (1988) 1665.

[8] L.F. Mattheiss and D.R. Hamann, Phys. Rev. B 38 (1988) 5012.

[9] S. Massidda, J. Yu and A.J. Freeman, Physica C 152 (1988) 251.

[10] M.S. Hybertsen and L.F. Mattheiss, Phys. Rev. Lett. 60 (1988) 1661.

[11] F. Herman, R.V. Kasowski and W.Y. Hsu, Phys. Rev. B 38 (1988) 204.

[12] I. Terasaki, S. Tajima, H. Eisaki, H. Takagi, K. Uchinokura and S. Uchida, Phys. Rev. B 41 (1990) 865.

[13] Y. Wang, G. Feng and A.L. Ritter, Phys. Rev. B 42 (1990) 420.

[14] Z.-X. Shen, P.A.P. Lindberg, I. Lindau, W.E. Spicer, C.B. Eom and T.H. Geball:, Phys. Rev. B 38 (1988) 7152.

[15] F.U. Hillebrecht, J. Fraxedas, L. Ley, H.J. Trodahl, J. Zaanen, W. Braun, M. Mast, H. Petersen, M. Schaible, L.C. Bourne, P. Pinsukanjana and A. Zettl, Phys. Rev. B 39 (1989) 236.

[16] A. Fujimori, Y. Tokura, H. Eisaki, H. Takagi, S. Uchida, and M. Sato, Phys. Rev. B 40 (1989) 730).

[17] A.E. Bocquet, S. Ogawa, H. Eisaki, H. Takagi, S. Uchida, A. Fujimori and S. Suga, Physica C 169 (1990) 1.

[18] C.G. Olson, R. Liu, D.W. Lynch, R.S. List, A.J. Arko, B.W. Veal, Y.C. Chang, P.Z. Jiang and A.P. Paulikas, Phys. Rev. B 42 (1990) 381.

[19] S. Berko, in: Positron Solid-State Physics, eds. W. Brandt and A. Dupasquier (North-Holland, Amsterdam, 1983) p. 64.

[20] L.P. Chan, D.R. Harshman, K.G. Lynn and D.B. Mitzi, Bull. Am. Phys. Soc. 35 (1990) 483.

[21] D. Singh, W.E. Pickett, R.E. Cohen, H. Krakauer and S. Berko, Phys. Rev. B 39 (1989) 9667.

[22] A. Bansil, R. Pankaluoto, R.S. Rao, P.E. Mijnarends, W. Dlugosz, R. Prasad and L.C. Smedskjaer, Phys. Rev. Lett. 61 (1988) 2480.

[23] A. Bansil, P.E. Mijnarends and L.C. Smedskjaer, Phys. Rev. B (in press).

[24] P.M. de Wolff, Acta Cryst. A 30 (1974) 777.

[25] A. Janner and T. Janssen, Phys. Rev. B 15 (1977) 643.

[26] T. Janssen and A. Janner, Adv. Phys. 36 (1987) 519.

[27] C. de Lange and T. Janssen, Phys. Rev. B 28 (1983) 195.

[28] S. Berko and J.S. Plaskett, Phys. Rev. 112 (1958) 1877.

[29] K. Kadowaki, M.J.V. Menken, A. Winkelman and A.A. Menovsky (private communication)

[30] P. Zwart, L.P.L.M. Rabou, G.J. Langedijk, A.P. Jeavons, A.P. Kaan, H.J.M. Akkerman and P.E. Mijnarends, in: Positron Annihilation, eds. P.C. Jain, R.M. Singru and K.P. Gopinathan (World Scientific, Singapore, 1985) p. 297.

[31] R.N. West, J. Mayers and P.A. Walters, J. Phys. E 14 (1981) 478.

[32] L.C. Smedskjaer and D.G. Legnini, Nucl. Instrum. and Methods A 292 (1990) 487.

FIGURE CAPTIONS

Fig. 1. Rocking curve for the (002) reflection with the [100] direction as rotation axis, measured by neutron diffraction.

Fig. 2. Contour diagram of the anisotropic part of the 2D-ACAR distribution measured at 6 K with integration along the c axis, after smoothing with a gaussian of FWHM = 0.375 mrad and C_{2v} symmetrization. Contours run from 0.1 to 1.0 arbitrary unit in steps of 0.1.

Fig. 3. Cuts along the $\underline{a}^*$ axis through the centres of the anisotropic parts of the 2D-ACAR distributions before C_{2v} symmetrization. a): T = 6 K; b): T = 92 K. The angle $\theta_y = p_y/(mcx10^{-3})$, where p_y is the y component of photon-pair momentum, m the electron mass and c the velocity of light. Data smoothed with a gaussian of FWHM = 0.375 mrad; five adjacent rows of channels parallel to the y direction have been added to increase statistics. Peaks and other structure have been labelled by their channel number (1 channel = 0.125 mrad); minus signs in front of channel numbers in the left halfs of the figures have been omitted for reasons of space.

Fig. 4. Cuts along the $\underline{b}^*$ axis through the centres of the anisotropic parts of the 2D-ACAR distributions before C_{2v} symmetrization. a): T = 6 K; b): T = 92 K. The angle $\theta_z = p_z/(mcx10^{-3})$. Otherwise as fig. 3.

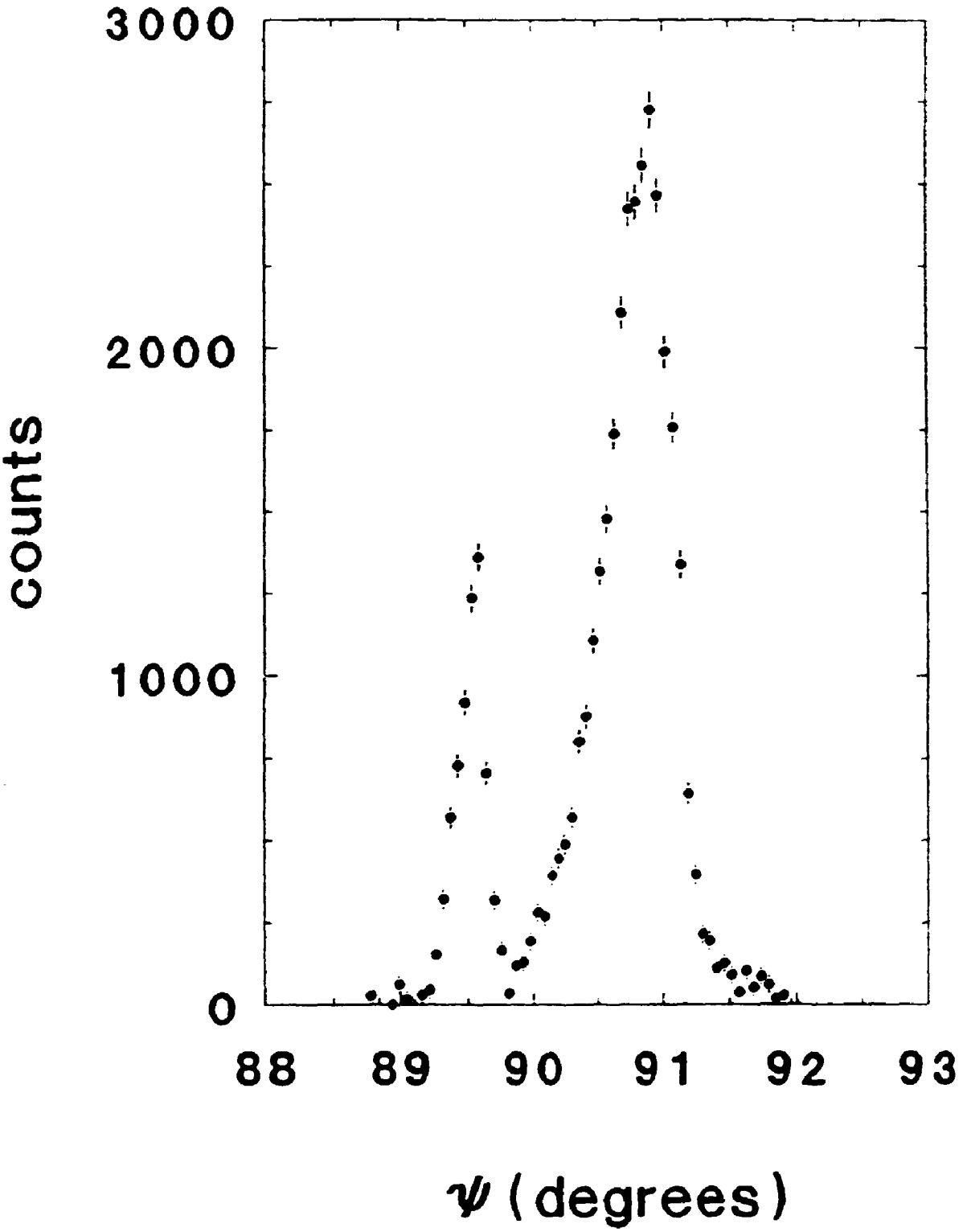

Fig. 1

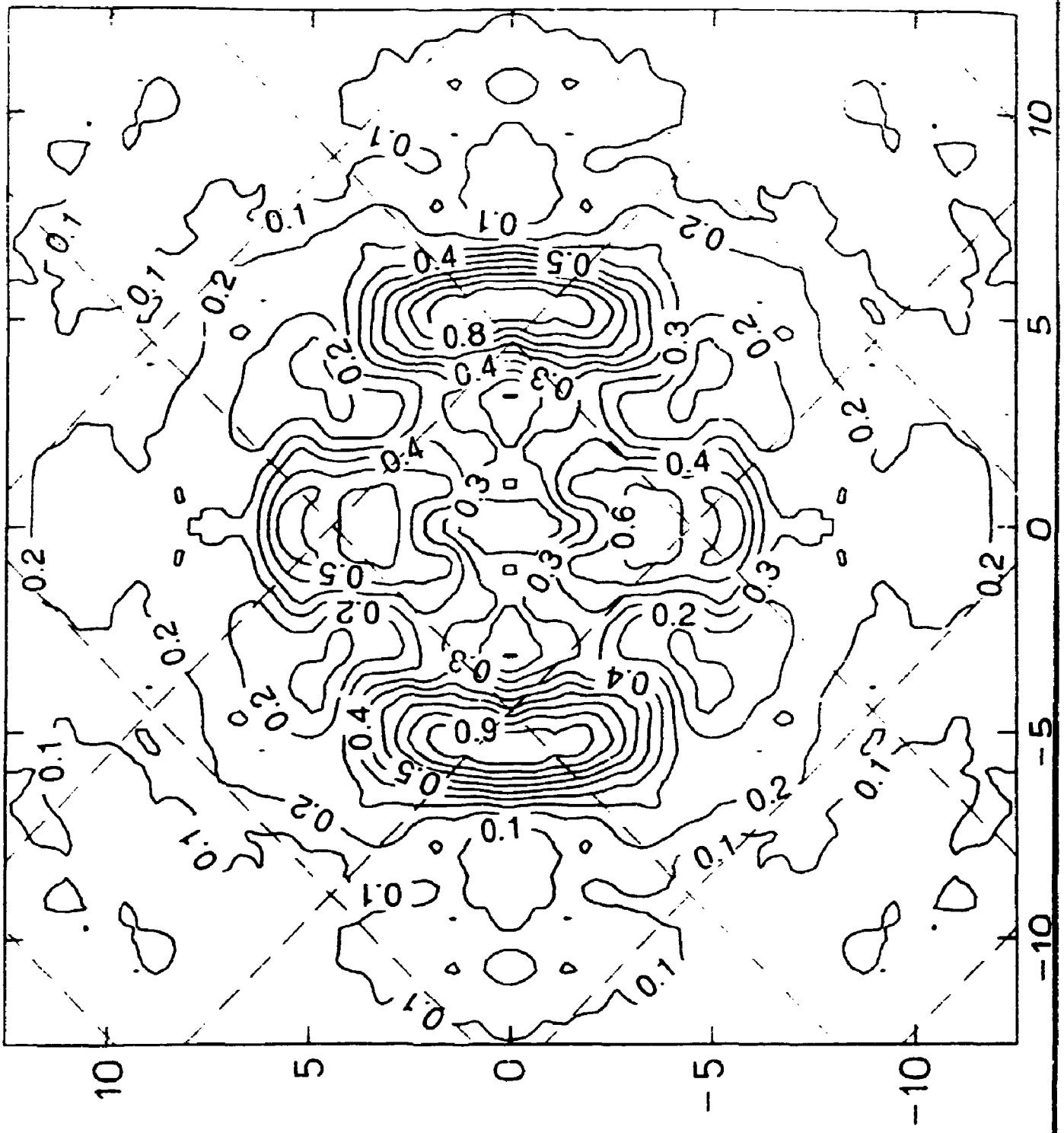

Fig. 2

Fig. 3a

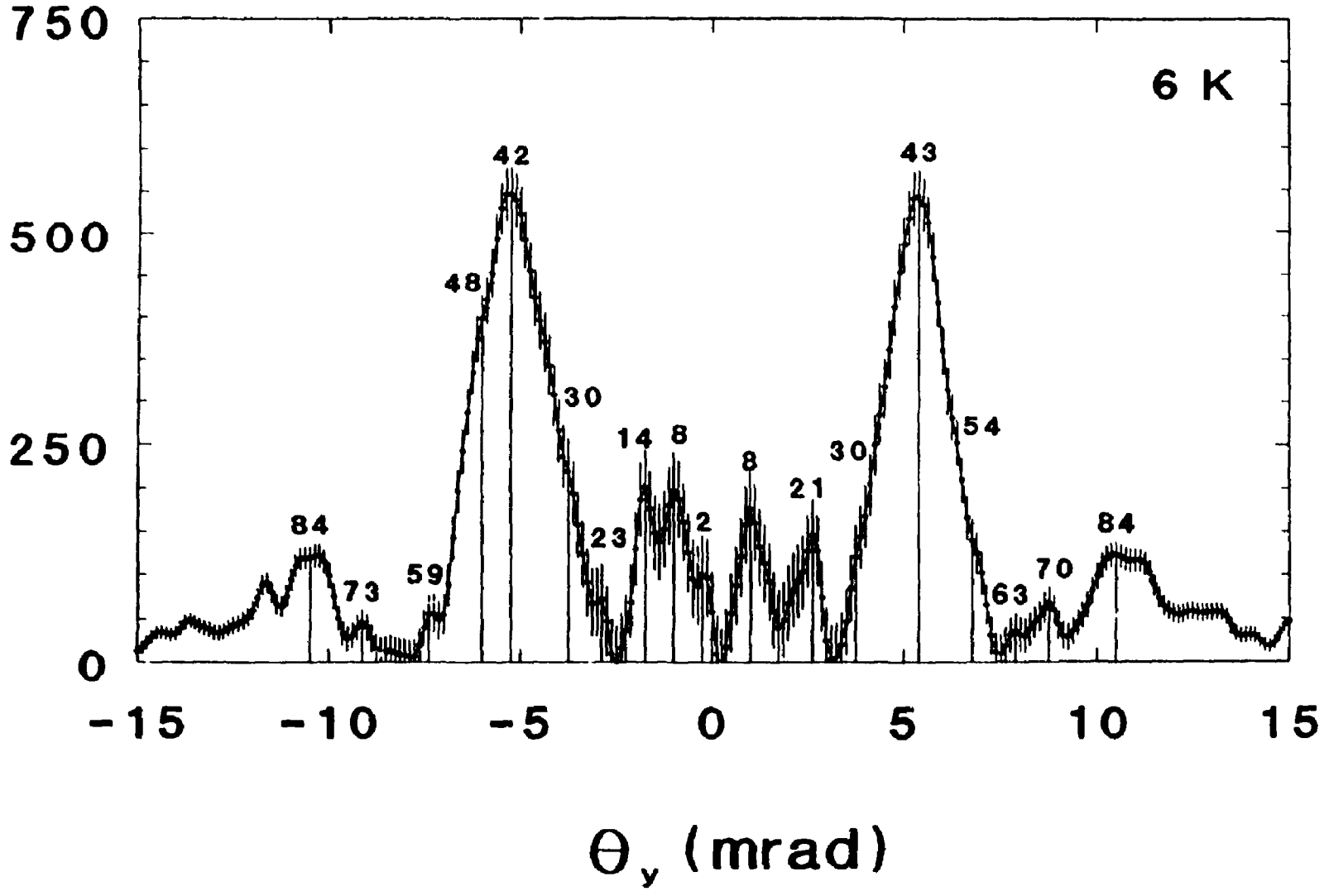
750
500
250
0
6 K
42
43
48
30
14
8
8
21
30
54
84
73
59
23
2
63
70
84
-15
-10
-5
0
5
10
15
Θ_y (mrad)

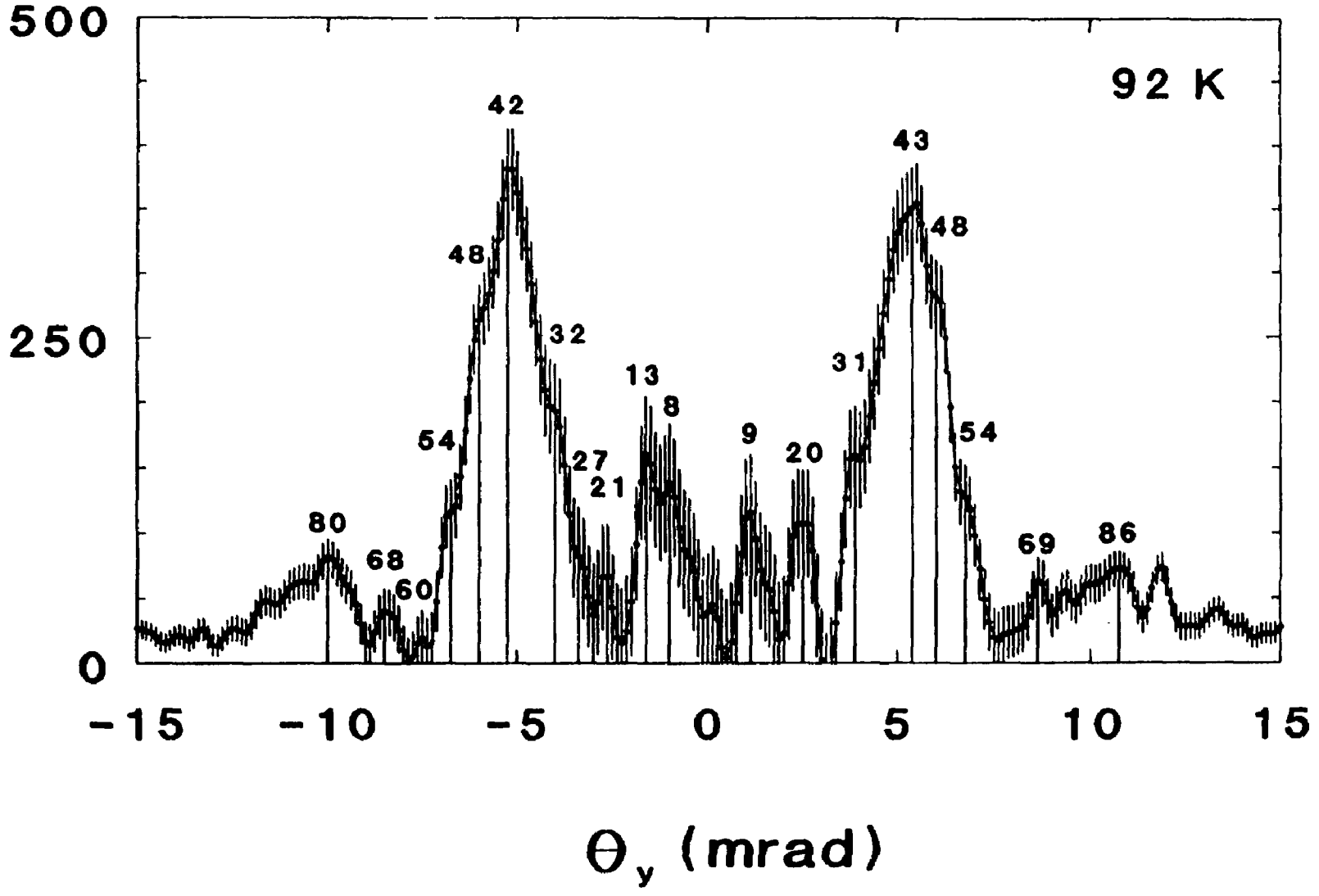
500
250
0
92 K
42
48
32
54
27
21
80
68
60
13
8
9
20
31
43
48
54
69
86
-15
-10
-5
0
5
10
15
Θ_y (mrad)

Fig. 3b

θ_y (mrad)

Fig. 4a

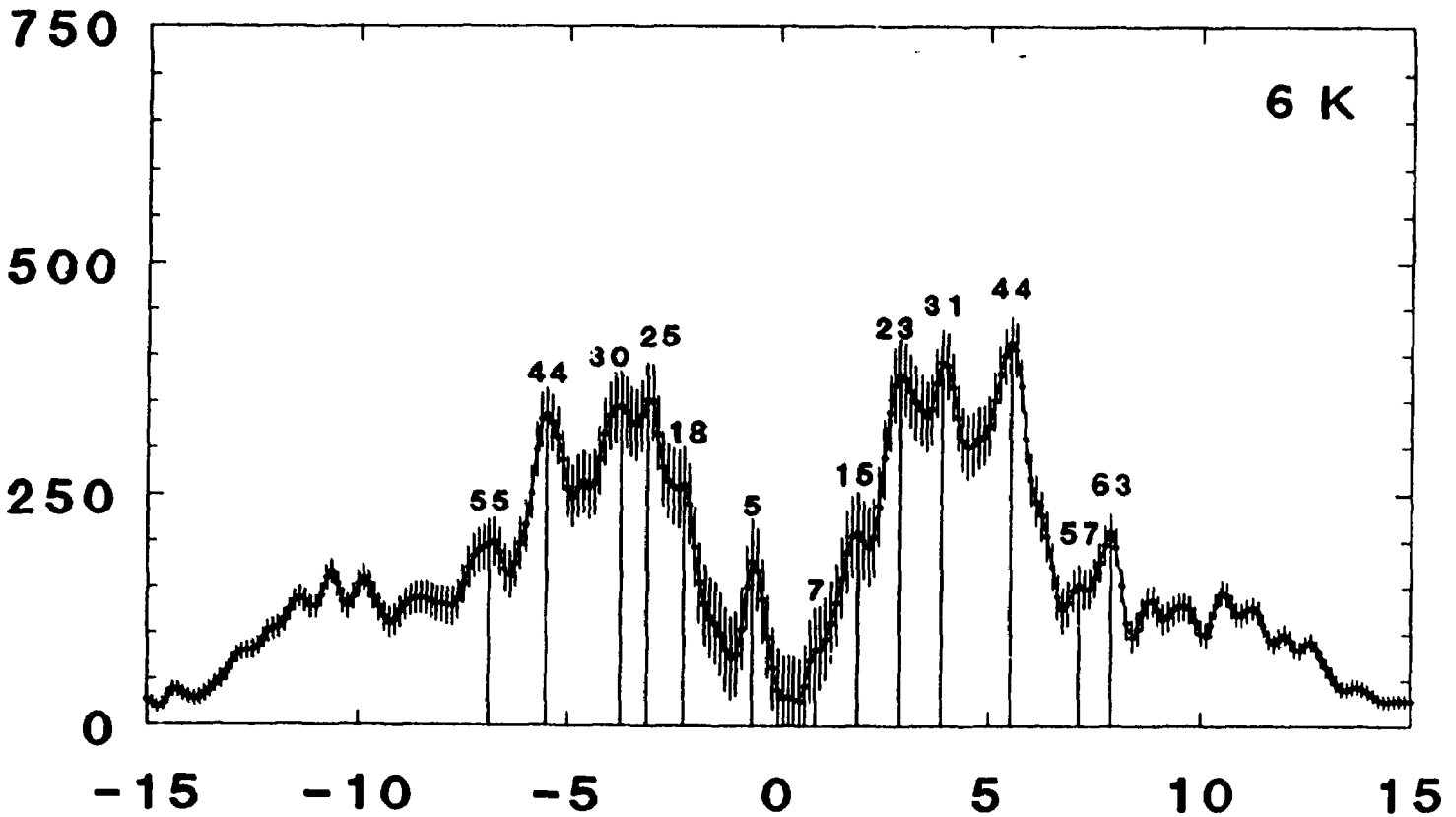

θ_z (mrad)

Fig. 4b

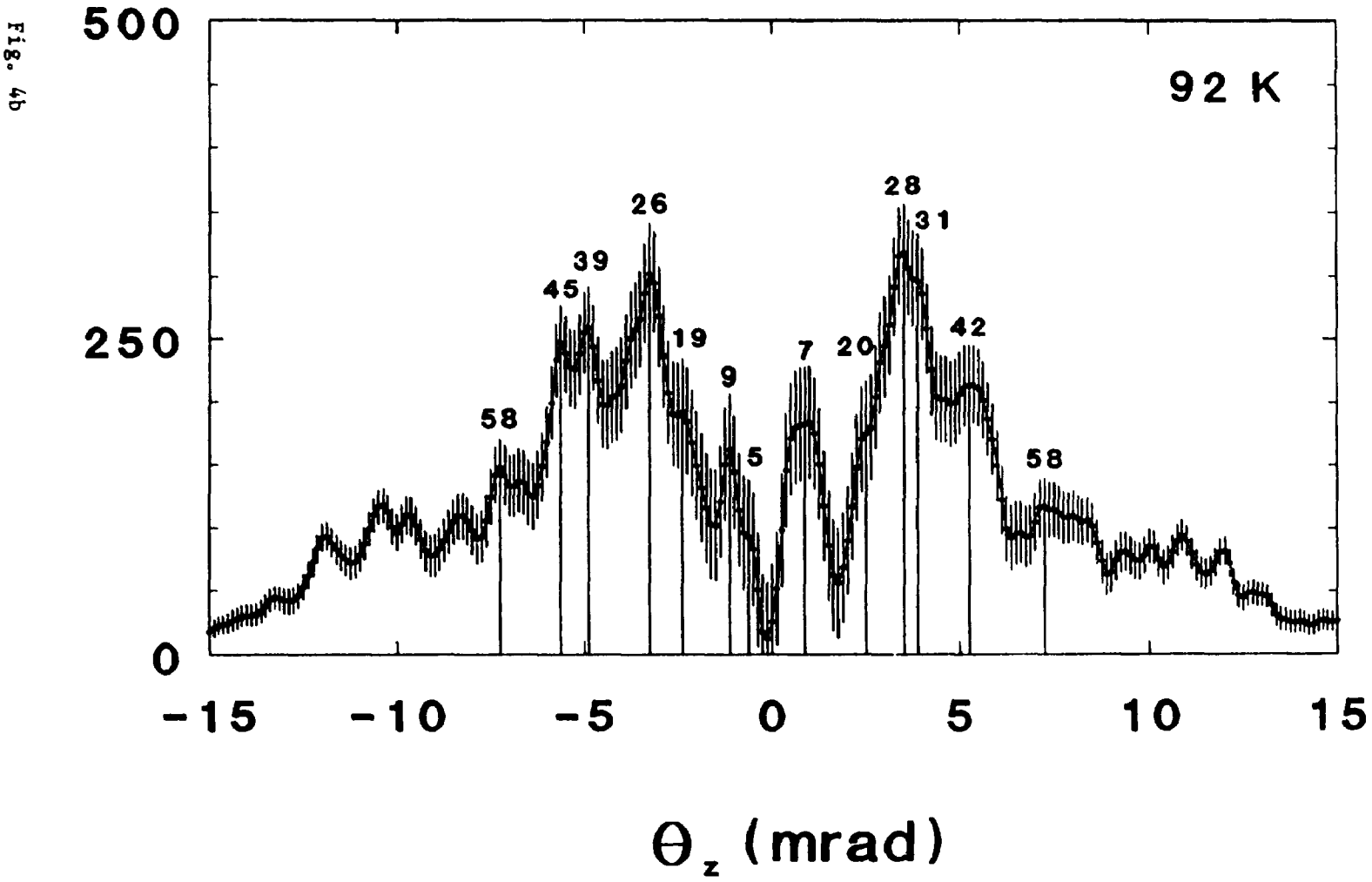
500
250
0
92 K
58
45
39
26
19
9
5
7
20
28
31
42
58
-15
-10
-5
0
5
10
15
θz (mrad)